Laser scanning microscopy of guided vortex flow in microstructured high-T_c films

A. Lukashenko and A. V. Ustinov
Physikalisches Institut III, Universität Erlangen-Nürnberg, Erwin-Rommel-Strasse 1, 91058 Erlangen, Germany

A. P. Zhuravel
Physikalisches Institut III, Universität Erlangen-Nürnberg, Erwin-Rommel-Strasse 1, 91058 Erlangen, Germany and B. Verkin Institute for Low Temperature Physics and Engineering, National Academy of Science of Ukraine, 47 Lenin Avenue, Kharkov 61103, Ukraine

E. Hollmann and R. Wördenweber[a)]
Institut für Schichten und Grenzflächen (ISG), Forschungszentrum Jülich, D-52425 Jülich, Germany and Center of Nanoelectronic Systems for Information Technology, Forschungszentrum Jülich, D-52425 Jülich, Germany

(Received 30 January 2006; accepted 17 May 2006; published online 31 July 2006)

We report the visualization of guidance of vortices by artificial microholes (antidots) in superconducting thin films using a low-temperature laser scanning microscope. Previously, guided motion of vortices via tilted rows of antidots in $YBa_2Cu_3O_7$ films was detected indirectly by using resistive Hall-type measurements. Here we prove that vortices are steered between antidots into *a priori* chosen direction by imaging of resistive photoresponse with a spatial resolution down to about 1 μm. We observe predominant paths for vortex motion. Vortices are nucleated and annihilated at antidots, i.e., antidots define starting and ending points of predominant vortex paths. Depending on the misorientation angle between rows of antidots and the current-driven direction of vortex motion, different channels dominate in antidot-guided vortex motion. Our experimental results can be explained by the *n*-channel model. Finally, we present direct measurements of the local critical currents. This technique can be used as a quantitative method for the analysis of vortex motion in micropatterned thin films. © *2006 American Institute of Physics*.
[DOI: 10.1063/1.2216819]

INTRODUCTION

With decreasing dimensions of a superconductor sample, formation and penetration of vortices and their interaction with each other and with the sample surface become increasingly important. One of the very effective ways to manipulate vortices in superconducting films is provided by the preparation of arrays of small micron-size holes which are often called antidots.[1] It has been shown that depending on the arrangement of antidots, flux trapping and guidance of vortices can be achieved via antidot patterns. Experiments indicate that the mechanism of flux transport depends upon the spacing of the holes.[2]

Imaging technologies are powerful tools to visualize and understand vortex motion in patterned superconductors. The low-temperature versions of scanning tunneling microscopy (STM),[3] magnetic force microscopy (MFM), scanning Hall probe microscopy,[4] laser scanning microscopy (LSM),[5] and magneto-optic[6] (MO) microscopy are complementary technologies for the visualization of vortices in superconductors. For instance, high resolution MFM and MO imaging are sensitive on the scale of the London penetration depth λ_L, whereas STM is sensitive to the variations of the order parameter ξ. However, these spatially resolving imaging techniques have very limited ability of imaging *moving* vortices. Investigations of the vortex dynamics in mesoscopic superconductors would greatly benefit from combining these techniques with LSM. The laser scanning technique allows for detailed mapping of vortex trajectories and dissipation paths.

The principle of LSM technique is similar to that of its "older sister," low temperature-scanning electron microscopy (LTSEM),[7] and based on mapping a sample voltage response as a function of the position of a focused laser beam (or electron beam, in case of LTSEM) on its surface. The LSM method requires a much simpler experimental setup than LTSEM, offers similar or better spatial resolution of the order of micron, generates less electromagnetic interference, and is inherently insensitive to magnetic fields.

The major effect of the laser beam on the sample during LSM imaging is local heating (bolometric response). There is also an additional (nonbolometric) contribution to the LSM response. In this case the light directly breaks Cooper pairs, creating nonequilibrium quasiparticles. The spatial resolution of the bolometric response is limited by the thermal healing length. The signal-to-noise ratios are greatly enhanced by modulating the power of the laser at some relatively low frequency f (typically, between 1 and 100 kHz) and measuring the response by a lock-in amplifier. The spatial resolution due to bolometric photoresponse mechanism increases with the frequency f because the effective thermal

[a)]Author to whom correspondence should be addressed; electronic mail: r.woerdenweber@fz-juelich.de

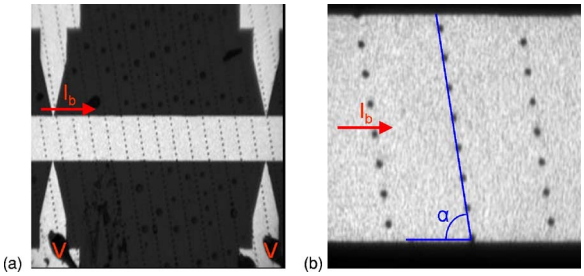

FIG. 1. LSM image obtained by measuring the intensity of laser beam reflected from the surface of sample 1: image of a 1000×1000 μm^2 sample area (a) and zoom into 200×200 μm^2 of sample area (b). In this sample the antidots (with a diameter of 5 μm measured via LSM) are spaced by 20 μm within the rows. The angle between the directions of antidot rows and bias current is $\alpha\approx81°$. The bright and dark regions correspond to the photoresponse obtained from the sample covered by Au film and the substrate, respectively.

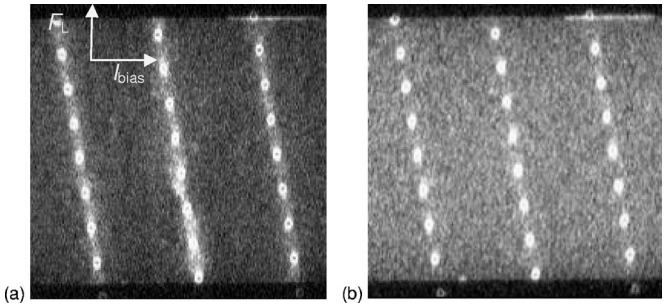

FIG. 2. LSM images obtained at temperature $T=86$ K by measuring the voltage response of sample 1 over the area of 200×200 μm^2. The critical current of the sample is $I_c=15$ mA. Images are taken at $I_{bias}=25$ mA $=1.7I_c$ (a) and $I_{bias}=95$ mA$=6.3I_c$ (b).

healing length shrinks. The nonbolometric component is frequency independent in the modulation frequency range that we use.

In this work, we apply low-temperature LSM technique to image guided motion of vortices in patterned high-T_c films. Indications for guided flux motion along rows of antidots have been previously obtained from Hall-type measurements of the flux transport in such films.[8] Here we directly prove that vortices are steered along rows of antidots. We also observe traces of "lost" vortices for small misorientation angle between rows of antidots and the direction of the bias current, i.e., large misorientation angles between the rows of antidots and the direction of the current-induced Lorentz force on the vortices.

SAMPLE PREPARATION

The samples were 100–200 nm thick $YBa_2Cu_3O_7$ films deposited on CeO_2 buffered r-cut sapphire by high-pressure magnetron sputtering. For protection of the superconducting film and in order to improve the contrast during photolithography, the $YBa_2Cu_3O_7$ films are covered with a 50 nm thick Au layer. The antidot arrays are patterned via optical lithography and ion beam etching at energy of 500 eV and a cooled substrate.[1] Figure 1 shows a typical arrangement of an antidot lattice in one of the studied samples. The direction of bias current (I_{bias}) with respect to the orientation of rows of antidots is defined by angle α.

EXPERIMENT

LSM measurements were done in the temperature range of 77–87 K in an optical cryostat. The accuracy of the temperature stabilization was better than ±0.05 K. Every sample was cooled down below its critical temperature $T_c\approx87$ K and biased at a dc current $I_{bias}\geqslant I_c$. Keeping the bias fixed, we scanned the sample surface by a focused laser beam (size of the focused beam of about 1 μm in diameter) and measured the resulting voltage δV change across the sample as a function of the laser beam coordinates. In order to decrease noise and improve spatial resolution we used a lock-in technique. The laser beam power was modulated at some frequency (usually from 1 up to 100 kHz) and the sample ac voltage response δV at this frequency was measured by a lock-in amplifier and recorded by a computer. To avoid any influence of the resistance of the bias wires all measurements were performed using the four-probe method.

The amplitude of the sample's photoresponse depends on the laser beam position as well as on other parameters such as laser beam intensity, modulation frequency, temperature of the sample, bias current, etc. An essential problem in these measurements compared to other typical LSM experiments was posed by the Au film covering the superconductor. The Au film had both very high reflectivity and shunted the $YBa_2Cu_3O_7$ film electrically which, in turn, resulted in a relatively low voltage response. Nonetheless, it was possible to visualize initiation and redistribution of resistive regions within the samples by changing and optimizing foregoing parameters, although the superconducting layer was covered with a shunting metal film having low electrical resistivity and high reflectivity.

Figures 2 and 3 show LSM images of two different samples with tilting angles $\alpha\approx81°$ for sample 1 (Fig. 2) and $\alpha\approx52°$ for sample 2 (Fig. 3). For each sample we obtained LSM images at different bias currents, first slightly larger than I_c and then well above I_c shown in Figs. 2(a) and 3(a) and Figs. 2(b) and 3(b), to respectively. Generally, brighter regions correspond to higher amplitudes of the voltage response δV. There is a number of interesting observations to be made.

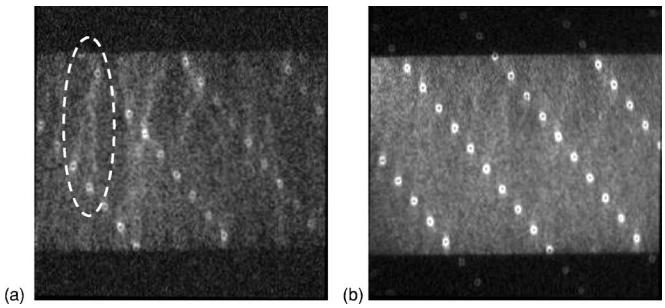

FIG. 3. LSM images obtained at temperature $T=86.5$ K by measuring voltage response of sample 2 over the area of 250×250 μm^2. The sample critical current is $I_c=6.5$ mA. Images are taken at $I_{bias}=8$ mA$=1.2I_c$ (a) and $I_{bias}=15$ mA$=2.3I_c$ (b). The dashed ellipsoid in (a) marks a position where two antidots of one row are connected via a bright line with one antidot of an adjacent row.

(i) The antidots show up as bright rings in the LSM images.
(ii) At low bias current, depending on the angle α, lines of higher brightness are visible either between the antidots in the rows or between the antidots of adjacent rows.
(iii) At high bias current the lines of high brightness disappear.

While the first observation is a more trivial artifact of the experiment, the second and third observations are indicative for the mechanism of guided motion of vortices. All observations are discussed in the following.

(i) In all images we observed a very intense voltage response induced by the focused laser beam around the antidots. The origin of this effect can be explained in the following way. The laser light gets scattered at the edges of antidots and is refracted in the transparent sapphire substrate. This scattered light is then reflected from the back of the substrate and shines back onto the superconducting film from below. Since the bottom of $YBa_2Cu_3O_7$ film is not covered by Au, it is black and thus light absorptive. This leads to an increase of the sample temperature and hence to a large LSM response around the edges of antidots. Thus, the high intensity at the edge of the antidot is an artifact of the measurement and not an indication for small critical properties in the vicinity of the antidot.
(ii) The bias current predominantly drives vortices in perpendicular direction, i.e., in our case from the bottom to the top of Figs. 2 and 3. At large bias current [$I_{\mathrm{bias}}=6.3I_c$ in Fig. 2(b) and $I_{\mathrm{bias}}=2.3I_c$ in Fig. 3(b)] depinning of vortices occurs over the whole sample. Due to the large driving force, vortices move throughout the sample, i.e., disregarding the small attractive potential of the antidots. This results in a homogeneous LSM photoresponse in the regions between antidots in the rows and the rows themselves. This is clearly visible in Figs. 2(b) and 3(b) where the LSM response is nearly uniform.
(iii) The most interesting case is represented by the images taken at small bias currents. At bias currents slightly exceeding I_c [$I_{\mathrm{bias}}=1.7I_c$ in Fig. 2(a) and $I_{\mathrm{bias}}=1.2I_c$ in Fig. 3(a)] the voltage response clearly visualizes predominant paths of vortex motion. In contrast to the situation of large driving forces where depinning of vortices occurs over the whole sample, for small driving forces and due to the attractive potential of the antidots, vortices will move predominantly from antidot to antidot.

The direction of vortex paths depends strongly on the angle α. For large angles ($\alpha\approx 81°$) the LSM response appears mainly along the rows of antidots [see Fig. 2(a)]. This indicates that vortices are nucleated at antidots and move from one antidot to the next in the row. For smaller angles as for sample 2 with angle $\alpha\approx 52°$ the situation is different [see Fig. 3(a)]. In this case, guided motion within the rows of antidots is not be detected by the LSM technique. However, bright lines between adjacent rows of antidots and oriented along the driving force become visible [see, for instance, the marked area in Fig. 3(a)]. This clearly indicates that vortices are also predominantly nucleated at and attracted by antidots. Thus, also in this case guidance of vortices by antidots is achieved. However, the driving force on vortices dominates their attraction to adjacent antidots in the row.

In a simple approach, it can be argued that the guided vortex motion can possibly be explained from a simple bottleneck principle by considering sample cross section within the rows of antidots, which depends on their size and angle α. The guided vortex motion sets in first for large antidots and small angle $90°-\alpha$ between the current-driven direction of vortex motion and antidot rows, when the sample cross section along the row of antidots is smaller than the cross section perpendicular to the bias current. In the opposite limit, i.e., small antidots and angle α significantly different from 90°, the cross section through antidots is large and guided motion does not occur. This simple approach, however, does not explain the dependence of vortex channel redistribution at higher bias currents and, especially, multiple vortex paths that are observed for smaller angles [see Fig. 3(a)] where a reduction of the current-carrying cross section by the presence of antidots is small.

Alternatively, observations of vortex motion guided by arrays of antidots can be explained by the "*n*-channel model" presented in Ref. 2. This model is based on the summation of flux transport in channels that are defined by the antidot array. In the simplest case (one-channel model) vortices are expected to drift predominantly along the "channel" defined by the rows of antidots. The component of the Lorentz force, which compels vortices to move along the antidot rows, is simply $F_{L,\mathrm{ch1}}=F_L \sin\alpha$, where F_L is the modulus of the Lorentz force, $F_L=|\boldsymbol{J}_{\mathrm{bias}}\times\boldsymbol{B}|$, with $\boldsymbol{J}_{\mathrm{bias}}$ and $\boldsymbol{B}$ the bias current density and the magnetic field, respectively. In case of large angles, $\sin\alpha\approx 1$ and predominant guided motion within this channel (the rows) is expected. This is the case for our sample 1 with $\alpha=81°$, as shown in Fig. 2(a). For smaller angles additional channels for vortex motion between antidots have to be taken into account. These additional channels are defined by the positions of adjacent antidots in neighboring rows. The probability of flux transport via these channels depends upon their geometrical orientation with respect to the driving force, i.e., the Lorentz force. In Ref. 2 the introduction of a second channel (two-channel model with the second channel defined by the geometrical orientation of closest antidot pairs in neighboring rows) was sufficient to exactly match the dependence of the flux transport upon the orientation of rows of antidots with respect to the driving force. However, a direct proof of the existence of additional channels for flux transport in arrays of antidots other than within rows of antidots has not been provided up to now. Our measurements clearly visualize the presence of a second channel for vortices motion due to the guidance of arrays of antidots. This is shown for sample 2 in Fig. 3(a). For an angle $\alpha\approx 52°$ the component of the Lorentz force $F_{L,\mathrm{ch1}}$ along the row is reduced by $\sim 20\%$. Vortices are generated at antidots and drift in the direction of the Lorentz force $\boldsymbol{F}_L$. Once they get close to the next row (distance between adja-

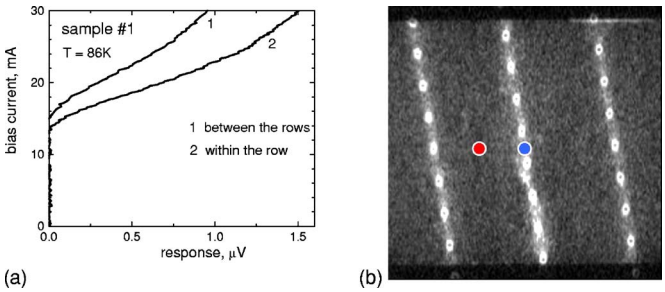

FIG. 4. (a) Amplitude of the voltage response δV induced by the focused laser beam as a function of the bias current I_{bias} in sample 1 at $T=86$ K. The red (1) and blue (2) curves are measured at two different positions of laser beam shown in picture (b). The red curve (1) is measured between the rows of antidots and the blue curve (2) is taken within the row.

cent rows are 60 μm), they feel the attractive potential of the nearest antidot. As a result, the path of vortex motion is terminated by that antidot.

Finally, we measured the dependence of the voltage response upon the bias current at fixed positions of the laser beam. These data are presented in Fig. 4. In this case, instead of scanning the whole surface, we focused the laser beam at some chosen position on the sample and varied the bias current I_{bias} through the sample. As an example, two sets of data are given in Fig. 4. The amplitude of the voltage response δV induced by the focused laser beam is recorded here for the laser spot placed between two antidots in a row and for the spot placed between two rows of antidots. The data demonstrate that, with increasing I_{bias}, the response appears first within the antidot rows [see curve 1 in Fig. 4(a)]. This indicates that vortex motion can more easily be stimulated within the rows of antidots than between rows. In a simplified picture, this situation could be characterized by two different critical currents, i.e., a smaller critical current $I_{c,\text{rows}}$ between antidots in a row compared to a larger critical current $I_{c,\text{bulk}}$ between adjacent rows. The difference in critical currents achieved by the micropatterning turns out to be of the order of 10% in the examined sample at 86 K. This method allows us to directly measure exact values for local critical current and, in a certain sense, a local *I-V* curve of any point of the sample. Our experiment yields quantitative values for the difference in the critical current encountered within a row of antidots as compared to the critical current between the rows. This technique can be used as a quantitative method for the analysis of vortex motion in micropatterned thin superconducting films.

CONCLUSIONS

We have performed LSM measurements on a superconducting $YBa_2Cu_3O_7$ thin film covered by a thin gold layer. In spite of the low electrical resistivity and the high optical reflectivity of the samples, we have been able to utilize full imaging capabilities of LSM.

We have visualized resistive regions caused by vortices moving in superconducting $YBa_2Cu_3O_7$ films with rows of antidots. We find that the spatial distribution of resistive regions depends on the angle α between rows of antidots and the direction of the bias current. In the case when α slightly differs from 90° ($\alpha \approx 81°$) the most favorable vortex motion direction at small bias current is along the antidot rows. At a gentler slope of antidot rows ($\alpha \approx 52°$) vortices preferably flow perpendicular to the bias direction at any current. These observations support the explanation of flux transport in micropatterned superconducting films in terms of the *n*-channel model.[2] Our measurements visualized more than one channel for flux transport in these systems. Vortices are nucleated at antidots and tend to drift in the direction of the Lorentz force $\boldsymbol{F}_L$. Once they get closer to the next antidot they feel the attractive potential of that antidot. For large angles α this next antidot is in the same row as the one where the vortex was nucleated; for smaller angle α the corresponding antidot is in the adjacent row. As a result, the paths of vortices are always originated and terminated by antidots. These measurements represent a clear visual proof of the presence of two alternative channels for vortices motion due to the guidance of arrays of antidots.

Finally, we demonstrate that the LSM method allows for a direct measurement of the local critical currents. Our experiment provided quantitative values for the difference in the critical current encountered within a row of antidots and the critical current of the superconducting film between the rows. This can be developed in a quantitative method for controlling the vortex manipulation in micropatterned thin films.

ACKNOWLEDGMENT

This work was supported by Deutsche Forschungsgemeinschaft (German Science Foundation).

[1] M. Baert, V. V. Metlushko, R. Jonckheere, V. V. Moshchalkov, and Y. Bruynseraede, Philips J. Res. **74**, 3269 (1995); A. M. Castellanos, R. Wördenweber, G. Ockenfuss, A. v. d. Hart, and K. Keck, Appl. Phys. Lett. **71**, 962 (1997); P. Selders and R. Wördenweber, Appl. Phys. Lett. **76**, 3277 (2000); R. Wördenweber, A. M. Castellanos, and P. Selders, *ibid.* **332**, 27 (2000); R. Wördenweber and P. Selders, *ibid.* **366**, 135 (2002).
[2] R. Wördenweber, P. Dymashevski, and V. R. Misko, Phys. Rev. B **69**, 184504 (2004).
[3] A. M. Troyanovski, J. Aarts, and P. H. Kes, Nature (London) **399**, 665 (1999).
[4] S. J. Bending, Adv. Phys. **48**, 449 (1999).
[5] D. Abraimov, D. M. Feldmann, A. A. Polyanskii, A. Gurevich, G. Daniels, D. C. Larbalestier, A. P. Zhuravel, and A. V. Ustinov, Appl. Phys. Lett. **85**, 2568 (2004).
[6] Ch. Jooss, J. Albrecht, H. Kuhn, S. Leonhardt, and H. Kronmüller, Rep. Prog. Phys. **65**, 651 (2002).
[7] R. Gross and D. Koelle, Rep. Prog. Phys. **57**, 651 (1994).
[8] R. Wördenweber and P. Dymashevski, Physica C **404**, 421 (2004).